SIViP (2016) 10:1481–1488
DOI 10.1007/s11760-016-0959-5

ORIGINAL PAPER

Range resolution improvement in FM-based passive radars using deconvolution

Musa Tunç Arslan[1] · **Mohammad Tofighi**[1] · **A. Enis Çetin**[1]

Received: 31 May 2016 / Revised: 27 July 2016 / Accepted: 1 August 2016 / Published online: 13 August 2016

Abstract FM-based passive bistatic radar (PBR) systems suffer from low range resolution because of the low baseband bandwidth of commercial FM broadcasts. In this paper, we propose a range resolution improvement method using deconvolution. The output of the PBR matched filter is processed using a deconvolution algorithm which assumes that targets are isolated, i.e., sparse in the range domain. The deconvolution algorithm is iterative and was implemented by performing successive orthogonal projections onto supporting hyperplanes of the epigraph set of a convex cost function. Simulation examples are presented.

Keywords Passive radar · Range resolution · Deconvolution

1 Introduction

PBR systems take advantage of an illuminator of opportunity, which is typically a commercial broadcast such as FM, DAB, DVB or GSM. Since commercial broadcasts are not intended for radar applications, PBR systems cannot change the transmitter characteristics or transmitted waveform for better radar performance [20]. Thus, one of the disadvantages of a PBR system is the detection range and range resolution, which is inversely proportional to the baseband bandwidth of the transmitted waveform. Often, the exploited waveform is an FM radio channel in PBR systems. However, baseband bandwidth of an FM signal is around 200 kHz. This low bandwidth heavily depends on the broadcast program and may result in a range resolution of 1.8–16 kms [3]. In other possible commercial broadcasts such as GSM, DAB or DVB, the range resolution is about 1.8, 0.2 and 0.044 km, respectively [3–6]. Unfortunately, they suffer from a lower detection range compared to FM due to transmitter characteristics [1–11]. Digital broadcasts address range resolution issue, especially DVB; however, the maximum detection range is limited compared to FM broadcast.

Multiple FM signals at different channels are used at the same time to overcome the low range resolution problem of FM-based PBR systems [2,17]. In [2,17], FM radio channels (and later DAB and DVB channels) are concatenated in the frequency domain to obtain a wide bandwidth illumination signal, the so-called multichannel FM signal. This approach increases the range resolution of a PBR system, but additional high amplitude peaks at the vicinity of target peaks are also generated as a side effect of matched filter processing.

In this paper, we propose a time-domain deconvolution scheme in order to increase the range resolution of a FM-based PBR system. The deconvolution algorithm is based on the projection onto convex sets theory [18]. In this algorithm, convex sets are hyperplanes which represent time delays of targets. In order to regularize the deconvolution process, orthogonal projections onto the epigraph set of ℓ_1-norm function are performed [4]. The ℓ_1-norm-based cost function assumes that the signals are sparse [5,8,13]. This assumption is justified because targets are isolated in space. Other deconvolution applications in radar signal processing include [21], in which authors increase the angular resolution.

The proposed method effectively increases the range resolution of single-channel FM-based PBR systems compared to the ordinary matched filter processing. It is also possible

This work was supported in part by the Scientific and Technical Research Council of Turkey, TUBITAK, under Project 113A010. Any opinion, determination and conviction are not the official opinion of TUBITAK in the publication according to the contract.

✉ Musa Tunç Arslan
mtarslan@ee.bilkent.edu.tr

[1] Department of Electrical and Electronics Engineering, Bilkent University, Ankara, Turkey

to apply this deconvolution scheme to multichannel FM-based PBR systems. Our algorithm can effectively suppress the sidelobes and increases the detection performance of the multichannel FM signal-based PBR system. The article is organized as follows. In Sect. 2, we describe how the matched filter output can be further processed to improve the range resolution of a PBR system. In Sect. 3, the application of the deconvolution algorithm onto the ambiguity function is presented. In Sect. 4, simulation examples are presented.

2 Ambiguity function and the deconvolution

The classical method of time of arrival estimation is based on the matched filter. The transmitted signal and the received signal are correlated using the ambiguity function. Naturally, transmitted waveform is not available directly in a PBR system unlike conventional radars. The PBR collects the transmitted waveform from a separate antenna. The surveillance signal is in the following form:

$$s_{\text{surv}}(t) = \sum_{p=1}^{P} a_p s(t-\tau_p)\mathrm{e}^{j2\pi f_p t} + a_s s(t-\tau_r) + \eta(t), \quad (1)$$

where $s(t)$ is the transmitted waveform, P is the number of targets in the coverage area, a_p is the complex attenuation coefficient of the signal echoing from pth target, f_p is the Doppler shift of the pth target, τ_p is the time delay of the signal echoing from the pth target, a_s is the complex attenuation coefficient of the direct signal received via the sidelobe of the surveillance antenna, τ_r is the distance between the transmitter and receiver, and $\eta(t)$ is the additive white Gaussian noise. The reference signal is a delayed version of the transmitted waveform:

$$s_{ref}(t) = a_r s(t-\tau_r), \quad (2)$$

where a_r is the complex attenuation coefficient of the transmitted signal and τ_r is the distance between the transmitter and receiver.

Since the reference antenna is directed to the transmitter, $s_{\text{ref}}(t)$ can have high SNR. The delay τ_r can be known in practice, so the effect of τ_r can be compensated by shifting the signal in time. In addition to this, the effect of the direct signal in the surveillance signal can be reduced considerably using beam-forming techniques at the surveillance antenna and adaptive filters [9]. We will assume that τ_r is equal to zero in the rest of this paper and the effect of the direct signal is considerably less compared to target echoes. The continuous-time ambiguity function $\xi(\tau, f)$ is defined as:

$$\xi(\tau, f) = \int_{-\infty}^{\infty} s_{\text{surv}}(t+\tau)s^*_{\text{ref}}(t)\mathrm{e}^{-j2\pi f t}\mathrm{d}t, \quad (3)$$

where τ is the time delay representing the range of the target and f is the Doppler shift. Matched filter is the optimal maximum likelihood receiver under the assumption of known P and additive white Gaussian noise [7]. However, the number of targets, P, is not known in practice. Additionally, the range resolution of the matched filter is limited by the main lobe of the autocorrelation of the transmitted waveform.

We now show that the ambiguity function defined in Eq. (3) can be expressed as the convolution of two two-dimensional (2-D) functions. With the assumption that the distance between transmitter and radar is known, we can substitute $\tau_r = 0$ into Eq. (3), and with beam forming and adaptive filtering, we can assume the effect of the direct signal can be diminished, and then using Eq. (1), we obtain

$$\xi(\tau, f) = \int_{-\infty}^{\infty} \left[\sum_{p=1}^{P} a_p s(t-(\tau_p-\tau))\mathrm{e}^{j2\pi f_p(t+\tau)} + \eta(t)\right] \times s^*(t)\mathrm{e}^{j2\pi f t}\mathrm{d}t \quad (4)$$

and with rearranging the summation, we obtain

$$\xi(\tau, f) = \sum_{p=1}^{P} a_p \mathrm{e}^{j2\pi f_p t} \int_{-\infty}^{\infty} s(t-(\tau_p-\tau)) \times s^*(t)\mathrm{e}^{j2\pi(f_p-f)t}\mathrm{d}t + \mu(\tau) \quad (5)$$

where the noise $\mu(\tau) = \int_{-\infty}^{\infty} \eta(t+\tau)s^*(t)\mathrm{e}^{-j2\pi f t}\mathrm{d}t$ is now signal dependent. The ambiguity function produces peaks at (τ_p, f_p) locations whenever it matches the signal due to a target. That is why it is also called a matched filter. We rewrite Eq. (5) as follows:

$$\xi(\tau, f) = \sum_{p=1}^{P} a_p \mathrm{e}^{j2\pi f_p \tau} r(\tau-\tau_p, f-f_p) + \mu(\tau), \quad (6)$$

where

$$r(\tau-\tau_p, f-f_p) = \int_{-\infty}^{\infty} s(t-(\tau_p-\tau)) \times s^*(t)\mathrm{e}^{j2\pi(f_p-f)t}\mathrm{d}t \quad (7)$$

As a result, Eq. (6) can be re-arranged as a 2-D convolution:

$$\xi(\tau, f) = \sum_{p=1}^{P} a_p \mathrm{e}^{j2\pi f_p \tau}\delta(\tau-\tau_p, f-f_p) * r(\tau, f) + \mu(\tau), \quad (8)$$

where $r(\tau, f) = \int_{-\infty}^{\infty} s(t+\tau)s^*(t)\mathrm{e}^{-j2\pi f t}\mathrm{d}t$ and $\delta(\tau, f)$ is the 2-D Dirac delta function. The so-called channel impulse response

$$h(\tau, f) = \sum_{p=1}^{P} a_p \mathrm{e}^{j2\pi f_p \tau}\delta(\tau-\tau_p, f-f_p) \quad (9)$$

is a complex function whose magnitude has clear peaks at (τ_p, f_p) pairs. These peaks must be sharper than the peaks of the ordinary ambiguity function which is the left-hand side of Eq. (8). Both $\xi(\tau, f)$ and $r(\tau, f)$ can be computed from the observed signals $s_{surv}(t)$ and $s(t)$ using 1-D Fourier transforms. As a result, unknown time delays τ_p and Doppler frequencies f_p, $p = 1, 2, \ldots, P$ in Eq. (8) can be estimated from the channel impulse response, which can be determined using deconvolution.

In many practical cases, Doppler frequencies, f_p, can be accurately estimated from the ambiguity function. In such cases, only time delays τ_p need to be estimated from Eq. (8). As a result, the problem becomes a 1-D deconvolution problem.

3 Complex deconvolution

Most deconvolution algorithms are developed for real signals, but they can be extended to complex signals in a straightforward manner.

The deconvolution problem in Eq. (8) can be discretized and re-expressed as a matrix-vector product as follows:

$$\mathbf{e} = \mathbf{R}\mathbf{h} + \mu, \tag{10}$$

where $\mathbf{e}$ is the observation vector obtained from the ambiguity function values, $\mathbf{R}$ contains samples from $r(\tau, f)$, $\mathbf{h}$ represents the channel impulse response vector, and μ is the noise. Inverse or pseudo-inverse of the matrix $\mathbf{R}$ may not produce good results because of the noise. It is possible to estimate $\mathbf{h}$ using iterative algorithms. One of the these iterative algorithms [10] is based on the following equation:

$$\mathbf{h}_{i+1} = \mathbf{h}_i - \lambda(\mathbf{e} - \mathbf{r} * \mathbf{h}_i), \quad i = 0, 1, 2, \ldots \tag{11}$$

where $\mathbf{e}$ is the discretized version of the 2-D ambiguity function, i is the iteration number, λ is the convergence parameter, and $\mathbf{r}$ is the discretized version of $r(\tau, f)$. With an appropriate choice of λ, Eq. (11) converges in the absence of noise. Another related iterative algorithm can be obtained using the projection onto convex sets (POCS) framework [19] which is based on the following equation:

$$\mathbf{h}_{i+1} = \mathbf{h_i} + \lambda \frac{\mathbf{e}[n, m] - (\mathbf{r} * \mathbf{h}_i)[n, m]}{||\mathbf{r}||^2}\mathbf{r}, \tag{12}$$

where $\mathbf{e}[n, m]$ is the $[n, m]$th sample of the discrete ambiguity function $\mathbf{e}$ and $0 < \lambda < 2$ for convergence in the absence of noise. In one iteration cycle of projection, operations described in Eq. 12 are repeated for all $[n, m]$ values of the ambiguity function $\mathbf{e}$. Both Eqs. 11 and 12 may not converge under noise. They may oscillate. In order to obtain a robust performance under noise, the deconvolution process has to be regularized. Both of the above iterative algorithms can be regularized by projecting the iterates onto the epigraph set of a convex cost function, which can be selected as the ℓ_1 norm cost function. The choice of ℓ_1 norm instead of the ℓ_2 energy function is a good choice for this problem because the ambiguity function is sparse in practice [5,13]. Ideally, it is nonzero only at the P target locations.

Regularization using projection onto epigraph set of the ℓ_1 norm Deconvolution algorithms described in Eqs. 11 and 12 are regularized by performing orthogonal projections onto the epigraph set of the ℓ_1 norm (PES-ℓ_1) during iterations [18]. In this problem, the system is complex. Therefore, we only project the magnitude of the iterate $\mathbf{h}_i$ onto the epigraph set of the ℓ_1 norm. Phase of the iterate is saved, and the next iterate is simply constructed from the projection result and the saved phase. Let the current iterate be $\mathbf{h}_i$. As described above, only the magnitude $\mathbf{g}_i = |\mathbf{h}_i|$ is projected onto the epigraph set of ℓ_1 (PES- ℓ_1) norm:

$$C_1 = \left\{ \underline{\mathbf{g}} = [\mathbf{g}_i \quad z] \in \mathbb{R}^{L+1} : \sum_{l=1}^{L} |g[l]| \leq z \right\}, \tag{13}$$

where $\mathbf{g}_i$ is assumed to be L-dimensional in this paper. The vector $\underline{\mathbf{g}}$ is obtained by concatenating z at the end of vector $\mathbf{g}$. PES-ℓ_1 set is the set of vectors whose ℓ_1-norm is less then or equal to some z. It is an upside-down pyramid in $L + 1$-dimensional space, and it is a closed and convex set [19]. Projection onto C_1 is obtained by the following equation:

$$\underline{\mathbf{g}}_{pi} = \underset{\underline{\mathbf{g}} \in C_1}{\operatorname{argmin}} ||\underline{\mathbf{g}} - \underline{\mathbf{g}}_i||^2, \tag{14}$$

where $\underline{\mathbf{g}} = [\mathbf{h} \quad 0]$ is in $\mathbb{R}^{L+1}$ and $\underline{\mathbf{g}}_{pi}$ is the projection of $\underline{\mathbf{g}}_i$ onto the epigraph set of ℓ_1-ball. The solution $\mathbf{g}_{pi}$ becomes sparser than $\mathbf{g}_i$ because the projection removes small-valued coefficients of vector $\mathbf{g}_i$. As pointed above, only the magnitude $\mathbf{g}_i$of the $\mathbf{h}_i = \mathbf{g}_i \exp(j\phi)$ is projected onto the set C_1. After the projection, the phase of the $\mathbf{h}_i$ is combined with $\mathbf{g}_{pi}$ and the next iterate $\mathbf{h}_{pi} = \mathbf{g}_{pi} \exp(j\phi)$ is obtained. Equation (12) is actually an orthogonal projection onto a hyperplane $C_{n,m}$ representing the set of $\mathbf{h}$ vectors which can produce the $\mathbf{e}[n, m]$ value of the ambiguity function $\mathbf{e}$ at the $[n, m]$ pair. In this paper, iterations described in Eq. (12) [or Eq. (11)] are combined with the regularization step described in Eq. (14). After one cycle of projections onto all $C_{n,m}$ sets, an orthogonal projection onto C_1 is performed. This cyclical process is repeated until the convergence is achieved. POCS theory states that iterates converge to a solution $\mathbf{h}^\star$ which is in the intersection of the sets $C_{m,n}$ and C_1 provided that the intersection set is non-empty. In practice, iterations are stopped either after several projection rounds or when the minimum mean square error $||\mathbf{h}_{i+1} - \mathbf{h}_i||$ is below a predefined threshold (Fig. 1).

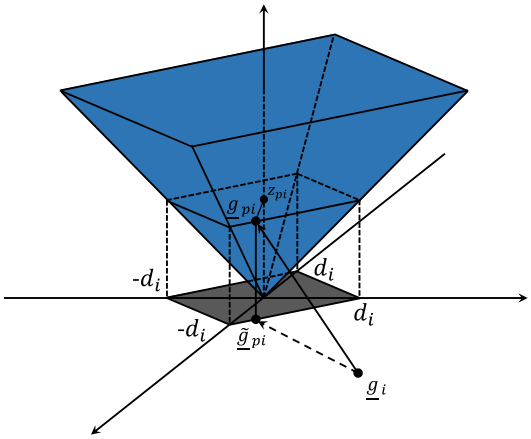

Fig. 1 Regularization using projection onto epigraph set of ℓ_1 norm. Graphical representation in $\mathbb{R}^3$ [4]

4 Simulation examples

We consider a simplified bistatic radar geometry in which there is one transmitter and one receiver which are both colocated. We assume that FM channels are all transmitted from one antenna site that includes several clustered antennas in close proximity. We generate the FM signals according to references [12,16]. Three different set of experiments are conducted.

First experiment set includes only two targets, and we investigate the amount of improvement deconvolution algorithms introduced to the system in the range resolution department.

In the second experiment, we investigate the performance of deconvolution algorithms with multichannel FM signals. Multichannel FM signals are an efficient proposal to overcome the range resolution problem of FM-based PBR systems; however, the ambiguity function is cluttered by many powerful sidelobes as a by-product of the ambiguity function. We expect deconvolution algorithms to suppress these sidelobes and improve the performance of the multichannel FM signal-based PBR systems.

In the last experiment set, the performance of the deconvolution approach is inspected under a crowded scenario with many targets and clutters.

We compare matched filter with three deconvolution algorithms: iterative deconvolution in Eq. (11) with PES-ℓ_1, POCS algorithm in Eq. (12) with PES-ℓ_1 and a well-known 2-D deconvolution algorithm, Lucy–Richardson method [15]. In the first simulation example, two targets, one at 10 km bistatic range and the other at 25 km bistatic range, are considered with SNRs -10 and -13 dB respectively. The Doppler f_p is the same, 25 Hz, for both targets. The target at 25 km gradually approaches to the target at 10 km to investigate the limits of the deconvolution algorithms and the ambiguity function. The start and end of the scenario is in Table 1.

Table 1 Start and end scenarios for the first experiment

		Bistatic range (km)	Doppler shift (Hz)	SNR (dB)
Start positions	$target_1$	10	25	-10
	$target_2$	25	25	-13
	Direct signal	NA	NA	30
Stop positions	$target_1$	10	25	-10
	$target_2$	17	25	-11
	Direct signal	NA	NA	30

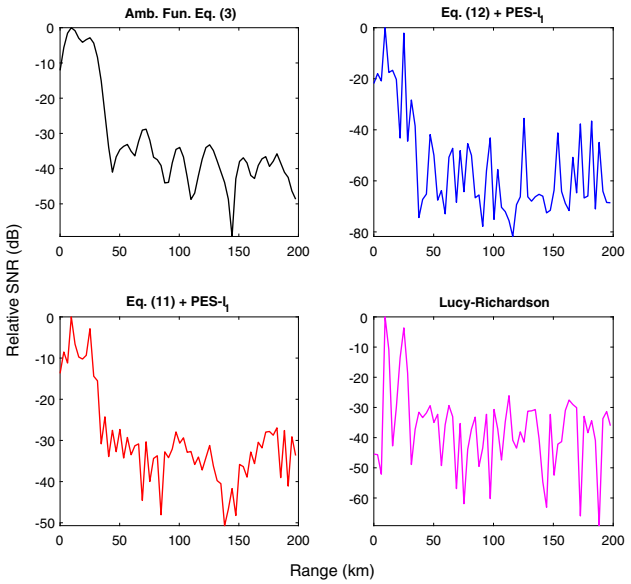

Fig. 2 Experimental results for two targets, one at 10 and the other at 25 km, respectively. 25 Hz Doppler frequency line

Experimental results are shown in Fig. 2. Only the $f_p = 25$ Hz line of the two-dimensional ambiguity function is plotted in Fig. 2. When there is 15 km distance between the two targets, the matched filter is barely able to separate the targets from each other. There is a 5 dB dip between the two targets [14]. However, deconvolution-based algorithms can clearly separate the targets with a 15 dB dip. When the distance between the two targets is 7 km, the results are shown in Fig. 3. The matched filter can no longer separate the targets. On the other hand, the deconvolution-based algorithms can still separate the targets with a more than 3 dB dip between the two targets. In Fig. 3, peaks due to targets are no longer as sharp as Fig. 2. In Fig. 3, the best result is obtained when the POCS deconvolution algorithm Eq. 12 is combined with the regularization scheme of PES-ℓ_1.

In Table 2, target separation distances of various methods are summarized. The best result (7 km) is obtained when Eq. 12 is combined with the PES-ℓ_1 regularization scheme.

It can even increase the range resolution of the PBR system up to 7 kms, which is about two times better than the ordinary

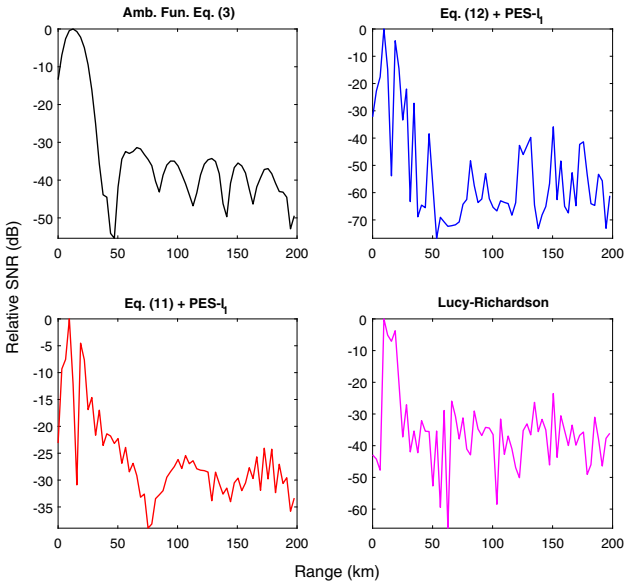

Fig. 3 Experimental results for two targets, one at 10 and the other at 17 km, respectively. $f_p = 25$ Hz Doppler frequency

Table 2 Performance of various methods for a single-channel FM case

	Algorithm	Dip level (dB) between targets	Target SNRs (dB) (# 1, # 2)
Target distance: 15 km $f_p = 25$ Hz	Amb. Func. Eq. (3)	−5	−10/−13
	Eq. (11)	−7	−10/−13
	Eq. (12)	−12	−10/−13
	Eq. (11) + PESℓ_1	−10	−10/−13
	Eq. (12) + PESℓ_1	−16	−10/−13
	Lucy–Rich.	−20	−10/−13
Target distance: 7 km $f_p = 25$ Hz	Amb. Func. Eq. (3)	0	−10/−13
	Eq. (11)	−3	−10/−13
	Eq. (12)	−5	−10/−13
	Eq. (11) + PESℓ_1	−20	−10/−13
	Eq. (12) + PESℓ_1	−35	−10/−13
	Lucy–Rich.	−9	−10/−13

ambiguity function Eq. (3). We experimentally observed that targets closer than 7 kms are not separated by any of the deconvolution algorithms.

In the second set of examples, we use multichannel FM signals as the illuminator of opportunity. We use three FM channels in all simulation examples with each FM channel having 200 and 100 kHz distance from each other in the frequency domain. In addition to the effect of deconvolution, we also investigate the effect of channel separation in this experiment. Some examples of spectrum of multichannel FM signals with 3 channels with different channel spacing are shown in Fig. 4.

We assume that there are two targets: one at 10 km and the other at 14 km away from the radar with SNRs 10 and

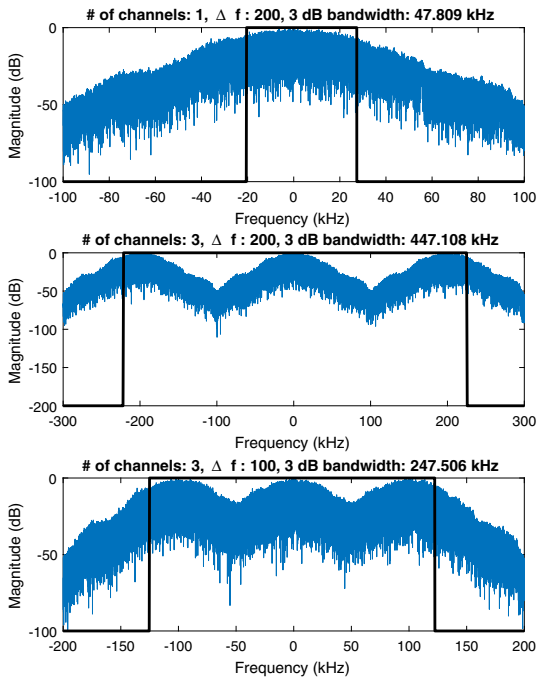

Fig. 4 Spectrum of a signal with single FM channel (*top*), a multichannel FM signal with 3 FM channels and 200 kHz channel spacing (*middle*), and a multichannel FM signal with 3 FM channels and 100 kHz channel spacing (*bottom*)

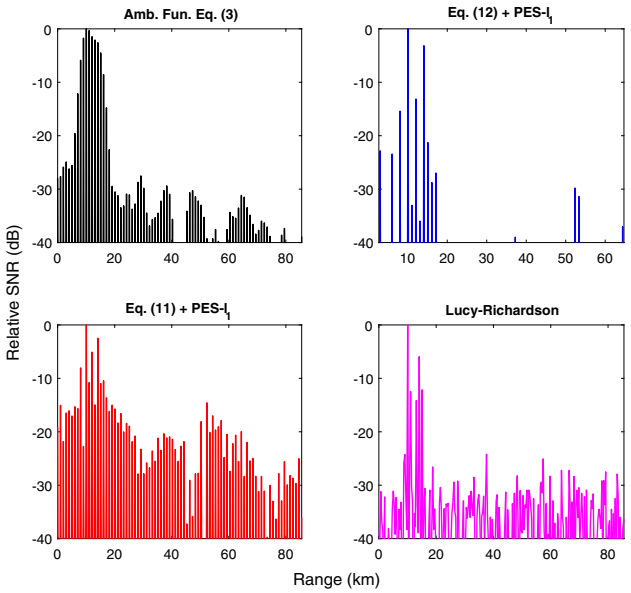

Fig. 5 Experimental results for two targets: one at 10 km and the other at 14 km for a multichannel scenario with 3 FM channels and channel space 200 kHz; 20 Hz Doppler frequency line

11 dB, respectively. Since the theoretical bandwidth is three times that of the single- channel FM case, it is possible to resolve targets even when there is a 4 km distance between them compared to the single-channel FM signal case. However, it is known that the multichannel FM case has spurious

peaks compared to the single-channel case at the output of the matched filter [17]. These peaks consist of actual target peaks and unwanted sidelobes. Due to the high amplitude of sidelobes, it is not possible to distinguish which peaks belong to the target and which peaks belong to the sidelobes in the ordinary ambiguity function. It is possible to observe that iterative deconvolution algorithms suppress most of the sidelobes as shown in Fig. 5. The iterative algorithm of Eq. (12) with PES-ℓ_1 suppresses the side lobes to about -14 dB which is a significant improvement over the other iterative deconvolution algorithms. The 2-D Lucy–Richardson algorithm also successfully suppresses the sidelobes to about -9 dB. The ambiguity function Eq. (3) has also two peaks, but the peaks are not sharp enough to determine the exact locations of targets.

In Fig. 5, when three FM channels with 200 kHz channel spacing are employed, the overall range resolution increases. However, due to the aforementioned powerful sidelobe problem with the ambiguity function, the targets are not distinguishable. There is only a -1.8 dB dip between the two peaks and they overlap. Due to the definition of resolving two close proximity targets in [14], in the multichannel scenario, the conventional ambiguity function could not resolve the two targets. However, the deconvolution algorithms are able to generate clean peaks by suppressing the sidelobes. Equation (12) with PES-ℓ_1 regularization determines the targets

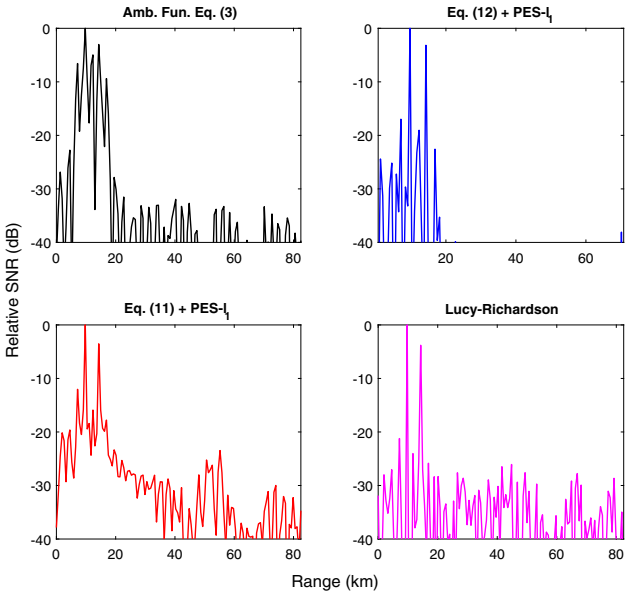

Fig. 6 Experimental results for two targets: one at 10 km and the other at 14 km for a multichannel scenario with 3 FM channels and channel space 100 kHz; 20 Hz Doppler frequency line

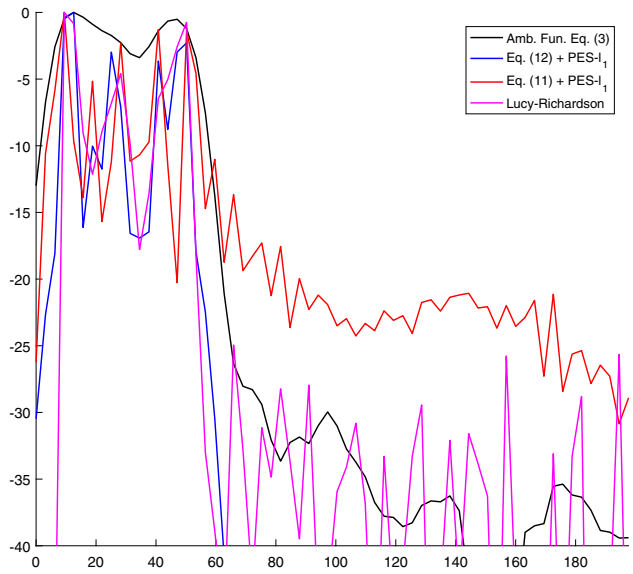

Fig. 7 Experimental results for five targets with a single FM channel system, 20 Hz Doppler frequency line

Table 3 Performance of various methods for a single-channel FM case

	Algorithm	# of targets resolved	Highest sidelobe level w.r.t. target (dB)	Target SNRs (dB) (# 1, # 2)
3 FM channels Δf: 200 kHz	Amb. Func. Eq. (3)	0	-1.8	$-11/-13$
	Eq. (11)	2	-3.8	$-11/-13$
	Eq. (12)	2	-6.8	$-11/-13$
	Eq. (11) + PESℓ_1	2	-5.8	$-11/-13$
	Eq. (12) + PESℓ_1	2	-13.8	$-11/-13$
	Lucy–Rich.	2	-6.8	$-10/-13$
3 FM channels Δf: 100 kHz	Amb. Func. Eq. (3)	2	-3.3	$-11/-13$
	Eq. (11)	2	-5.6	$-11/-13$
	Eq. (12)	2	-7.7	$-11/-13$
	Eq. (11) + PESℓ_1	2	-9.3	$-11/-13$
	Eq. (12) + PESℓ_1	2	-15.8	$-11/-13$
	Lucy–Rich.	2	-8.8	$-11/-13$

Table 4 Experimental results for the last experiment with both single- and multichannel FM signals

	Algorithm	# of targets resolved	Highest sidelobe level w.r.t. target (dB)	Target SNRs (dB) (# 1, # 2)
Single FM channel	Amb. Func. Eq. (3)	2	0	0/−2/−5 / −3/−5
	Eq. (11)	3	1	0/−2/−5/−3/−5
	Eq. (12)	3	2	0/−2/ −5/−3/−5
	Eq. (11) + PESℓ_1	4	3	0/−2/−5/−3/−5
	Eq. (12) + PESℓ_1	5	5	0/−2/−5/−3/−5
	Lucy–Rich.	3	3	0/−2/−5/−3/−5
3 FM channels Δf: 200 kHz	Amb. Func. Eq. (3)	5	5	0/−2/−5/−3/−5
	Eq. (11)	5	5	0/−2/−5/−3/−5
	Eq. (12)	5	5	0/−2/−5/−3/−5
	Eq. (11) + PESℓ_1	5	5	0/−2/ −5/−3/−5
	Eq. (12) + PESℓ_1	5	5	0/−2/−5/−3/−5
	Lucy–Rich.	5	5	0/−2/−5/−3/−5
3 FM channels Δf: 100 kHz	Amb. Func. Eq. (3)	5	5	0/−2/−5/−3/−5
	Eq. (11)	5	5	0/−2/−5/−3/−5
	Eq. (12)	5	5	0/−2/−5/−3/−5
	Eq. (11) + PESℓ_1	5	5	0/−2/−5/−3/−5
	Eq. (12) + PESℓ_1	5	5	0/−2/−5/−3/−5
	Lucy–Rich.	5	5	0/−2/−5/−3/−5

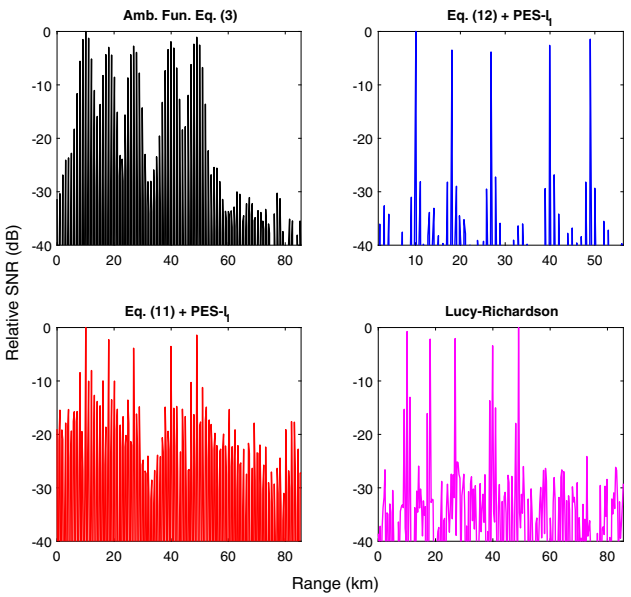

Fig. 8 Experimental results for five targets with a multichannel FM channel system with 3 FM channels and 200 kHz channel separation, 20 Hz Doppler frequency line

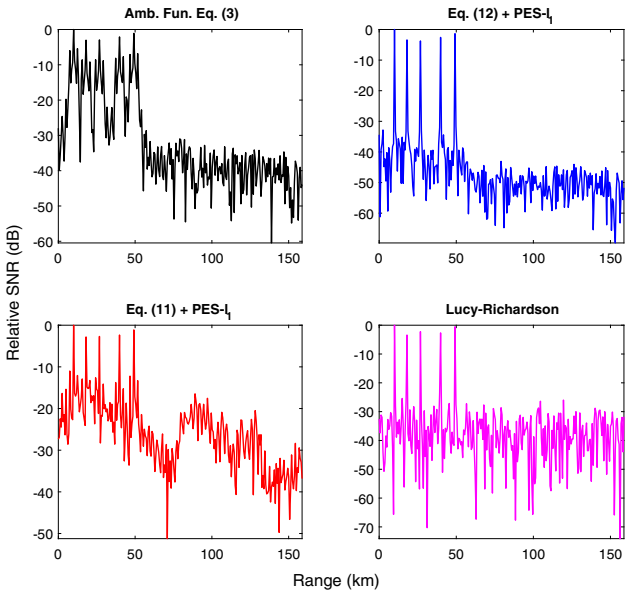

Fig. 9 Experimental results for five targets with a multichannel FM channel system with 3 FM channels and 100 kHz channel separation, 20 Hz Doppler frequency line

with a dip level of −13.8 dB for side lobes and is the best resulting deconvolution scheme.

The effect of channel spacing is shown in Fig. 6. Overlapping the FM channels so that the channel spacing is 100 kHz instead of 200 kHz decreased the overall sidelobe level at the output of the ambiguity function. However, this decrease in sidelobes is achieved with a trade-off of the overall range resolution. Since the channel spacing is 100 kHz, the overall bandwidth of the signal used is now narrower. With overlapping FM channels, the sidelobe levels decreased and the deconvolution schemes further enhance the performance of the ambiguity function by suppressing the sidelobe levels to the noise floor. A summary of this experiment is given in Table 3.

In the next experiment, there are five targets with ranges, 10, 18, 27, 40 and 49 kms, and the relative attenuation values compared to the most powerful target power are 0, −3, −3, −2 − 1 dB, respectively. In addition to the targets, there are 6 stationary objects (clutters) in the environment with ranges, 1, 3, 4, 8, 12 and 23 kms, and the relative attenuation values compared to the most powerful target power are 13, 10, 8, 10, 12 and 13 dB, respectively. The clutters are eliminated from the surveillance signal using an RLS adaptive filter [9]. All of the targets have the same $fp = 20$ Hz with a single-channel FM case. The experimental detection results are shown in Fig. 7. Equation (12) with PES-ℓ_1 regularization can find all targets. The ambiguity function is not able to find any of the actual target peaks. It only generates two peaks. Equation 11 with PES-ℓ_1 can resolve four targets. Other deconvolution methods can only resolve three of the targets. Experimental results are summarized in Table 4.

Equation (12) with PES-ℓ_1 regularization can find all targets. The ambiguity function is not able to find any of the actual target peaks. It only generates two peaks. Equation (11) with PES-ℓ_1 can resolve four targets. Other deconvolution methods can only resolve three of the targets. Experimental results are summarized in Table 4.

In Figs. 8 and 9, a multichannel FM signal with 3 FM channels with 200 and 100 kHz channel spacing, respectively, is employed on the same scenario. The targets can be easily distinguished, and even the ambiguity function is able to generate 5 separate target peaks with lower sidelobe levels in the 100 kHz channel spacing case as expected. However, there are many powerful sidelobe peaks around the target peaks in the 200 kHz channel spacing case. It can be observed that deconvolution algorithms are able to suppress these sidelobes significantly in both 200 and 100 kHz channel spacing.

5 Conclusion

A new complex deconvolution algorithm is proposed for PBR systems. The deconvolution algorithm is implemented as a post-processing method, and it is applied to the range-Doppler map output of the matched filter. In all the simulation examples that we tried, our deconvolution-based approach improves the target separation performance of the PBR system. The PES-based regularization during the deconvolution process further improves the target detection results. The proposed algorithm works for both single-channel FM and multichannel FM cases.

In addition to the FM-based PBR systems, this approach can be further extended to any radar system in order to improve the range resolution because the method is based on the exploitation of the well-known ambiguity function.

References

1. Baker, C., Griffiths, H., Papoutsis, I.: Passive coherent location radar systems. Part 2: waveform properties. IEE Proc. Radar Sonar Navig. **152**(3), 160–168 (2005)
2. Berger, C.R., Demissie, B., Heckenbach, J., Willett, P., Zhou, S.: Signal processing for passive radar using OFDM waveforms. IEEE J. Sel. Topics Signal Process. **4**(1), 226–238 (2010)
3. Bezoušek, P., Schejbal, V.: Bistatic and multistatic radar systems. Radioengineering **17**(3), 53 (2008)
4. Cetin, A.E., Tofighi, M.: Projection-based wavelet denoising. IEEE Signal Process. Mag. **32**(5), 120–124 (2015)
5. Deprem, Z., Cetin, A.E.: Cross-term-free time-frequency distribution reconstruction via lifted projections. IEEE Trans. Aerosp. Electron. Syst. **51**(1), 479–491 (2015)
6. Fabrizio, G., Colone, F., Lombardo, P., Farina, A.: Passive radar in the high frequency band. In: Radar Conference, 2008. RADAR'08, pp. 1–6. IEEE (2008)
7. Fuchs, J.J.: Multipath time-delay detection and estimation. IEEE Trans. Signal Process. **47**(1), 237–243 (1999)
8. Hadi, M.A., Alshebeili, S., Jamil, K., El-Samie, F.E.A.: Compressive sensing applied to radar systems: an overview. SIViP **9**(1), 25–39 (2015)
9. Howland, P.E., Maksimiuk, D., Reitsma, G.: Fm radio based bistatic radar. IEE Proc. IET Radar Sonar Navig. **152**, 107–115 (2005)
10. Katsaggelos, A.K., Schafer, R.W.: Iterative deconvolution using several different distorted versions of an unknown signal. In: Acoustics, Speech, and Signal Processing, IEEE International Conference on ICASSP'83., vol. 8, pp. 659–662. IEEE (1983)
11. Klein, M., Millet, N.: Multireceiver passive radar tracking. IEEE Aerosp. Electron. Syst. Mag. **27**(10), 26–36 (2012)
12. Lauri, A., Colone, F., Cardinali, R., Bongioanni, C., Lombardo, P.: Analysis and emulation of fm radio signals for passive radar. In: IEEE Aerospace Conference, 2007. IEEE, pp. 1–10 (2007)
13. Malioutov, D., Çetin, M., Willsky, A.S.: A sparse signal reconstruction perspective for source localization with sensor arrays. IEEE Trans. Signal Process. **53**(8), 3010–3022 (2005)
14. Richards, M.A.: Fundamentals of Radar Signal Processing. Tata McGraw-Hill Education, New York (2005)
15. Richardson, W.H.: Bayesian-based iterative method of image restoration. JOSA **62**(1), 55–59 (1972)
16. Several authors: Transmission standards for fm sound broadcasting at vhf. In: Rec. ITU-R BS.450-3, ITU (2001)
17. Tasdelen, A.S., Koymen, H.: Range resolution improvement in passive coherent location radar systems using multiple fm radio channels. IET (2006)
18. Tofighi, M., Kose, K., Cetin, A.: Denoising using projections onto the epigraph set of convex cost functions. In: IEEE International Conference on Image Processing (ICIP'14) (2014). doi:10.1109/ICIP.2014.4379511
19. Tofighi, M., Yorulmaz, O., Kose, K., Yildirim, D., Cetin-Atalay, R., Cetin, A.: Phase and tv based convex sets for blind deconvolution of microscopic images. IEEE J. Sel. Topics Signal Process. **10**(1), 81–91 (2016). doi:10.1109/JSTSP.2015.2502541
20. Wang, L., Gao, F., Xu, J., Wang, D., He, M., Yuan, J.: Orthogonal wideband hybrid-coding radar waveforms design. Signal Image Video Process. (2016). doi:10.1007/s11760-016-0905-6
21. Zha, Y., Huang, Y., Sun, Z., Wang, Y., Yang, J.: Bayesian deconvolution for angular super-resolution in forward-looking scanning radar. Sensors **15**(3), 6924–6946 (2015)